Proximity effects in superconducting spin-valve structures

Flokstra, M.G.

Chapter 5

Superconducting spin-valve: strong ferromagnetic case

5.1 Introduction

To grasp the differences between the weak ferromagnetic based spin-valves, as discussed in the previous chapter, and the strong ferromagnetic based spin-valves, which are the main ingredient of this chapter, let us start by highlighting the key aspects of the former, in particular, the mechanisms involved in the working of the spin-valve device. The term "weak" in this context means not only that the ferromagnetic exchange energy $E_{\rm ex}$ is much smaller than the Fermi energy E_F, but additionally assumes identical spin bands (to achieve zero spin polarization) and neglects contributions from the dipolar fields generated by the magnetization resulting from $E_{\rm ex}$. These two assumptions seem to be reasonable for small and homogenous exchange field $H_{\rm ex}$, and for these systems, experimental data confirm the theoretical predictions [48, 49]. For the spin-valve system in the weak limit with homogeneous $H_{\rm ex}$, the driving mechanism that leads to the T_c difference between the parallel (P) and anti-parallel (AP) alignment of the exchange fields, is based on enhanced dephasing of the induced pairs in P alignment. This originates from the momentum difference the induced pair obtains if the system is in P alignment, which it does not obtain in AP alignment (see Fig. 4.2). The enhanced dephasing causes a lowering of the Cooper pair density near the interface which leads to a T_c lowering. Inhomogeneities in $H_{\rm ex}$, especially in the form of magnetic domains and domain walls, make that at a single S/F interface anti-parallel regions exist. The alignment is no longer purely parallel, and all the non-parallel fractions/regions contributes to a T_c enhancement. It is still the Cooper pair which needs to provide this coupling (and sample different directions of the exchange fields) and therefore, just as in the spin valve where the two F layers should not be separated more than a few times the superconducting coherence length ξ_S, the distance over which the inhomogeneity should appear (to make a difference) is also limited to a few times ξ_S. The use of weak limit theory is actually a forced restriction. The theoretical framework based on the quasi-classical Green functions is unable to deal with correlation between particles which are separated by energies of the order of E_F. This limit the models to ferromagnets with $E_{\rm ex} \ll E_F$. Secondly, incorporating non-identical spin-bands (to deal with polarization) into the model gives severe mathematical difficulties, and thus identical (normal metal) spin bands are used, which is another reason to remain in the limit for weak ferromagnetism. What can be included are dipolar fields and inhomogeneities, and especially the latter has been included in the form of domain walls in S/F [41] or non-collinear magnetization in spin-valves [67]

In the previous chapter we studied Nb/CuNi devices, and in particular

the influence of the domains on the superconducting state. We found a contribution from these domains equally important as that from the P versus AP state in real spin-valve devices. However, a dominant contribution from dipolar fields, generated by those domains, was not found in any of the devices. In this chapter we continue this study on Nb/Py spin-valves, where the dipolar fields are much stronger. As we will show, in these devices the dipolar fields may become a dominant contribution and couple the magnetic states of both the Py layers in the spin-valve. Before we show the results obtained on the various devices, we first discuss what the effects of non-identical spin bands, encountered in "real" (or strong) ferromagnetic materials, on the superconducting spin-valve will be, on a qualitative level.

5.2 Polarized spin bands

We consider a thin layered F/S/F spin-valve in the dirty limit (i.e. all relevant length scales are much longer than the electron mean free path). The ferromagnets are homogeneously magnetized (single domain) and the exchange fields of the two ferromagnets are directed along the interfaces in either a parallel (P) or anti-parallel (AP) configuration. The dipolar fields of the ferromagnets are assumed to be much lower than $H_{c\|}$ (the parallel critical field strength) and do not affect the superconducting state (i.e. their pair breaking strength is zero). The exchange energies of the ferromagnets are neither in the so called weak-limit ($E_{\rm ex} \ll E_F$) or the strong-limit ($E_{\rm ex} \sim E_F$), so we have $E_{\rm ex} < E_F$. As a result, the spin bands cannot considered to be identical (weak limit) or decoupled ("perfect" strong limit). This, in consequence, gives rise to a spin dependent density of states, Fermi velocity, diffusion constant, etc. The (much) increased strength of the exchange field, compared to the weak limit, results in an enhancement of the suppression of the superconducting state. However, there is also an opposite effect due to the polarization of the spin bands. The Andreev reflections at a single interface become suppressed due to the presence of the minority spin band, more Cooper pairs are confined inside the superconductor, and the polarization therefore leads to a *reduced* suppression of the superconducting state. For the spin-valve, the essential process is the *crossed* Andreev reflection, in which the two electrons of the pair are removed in the opposite ferromagnetic banks. In the P configuration this always includes a minority spin band, while in the AP configuration both electrons can be accomodated in the majority bands. This means the AP configuration is now less confining and more efficient as pair breaker. In the limit of full spin polarization Cooper pairs have become fully confined in the P configuration, but still *can* leave the superconductor by crossed Andreev

reflections in the AP configuration. In other words, for weak magnets the P configuration suppresses superconductivity more strongly, but in the case of strong spin polarization it is the AP configuration, opposite to the weak limit result!

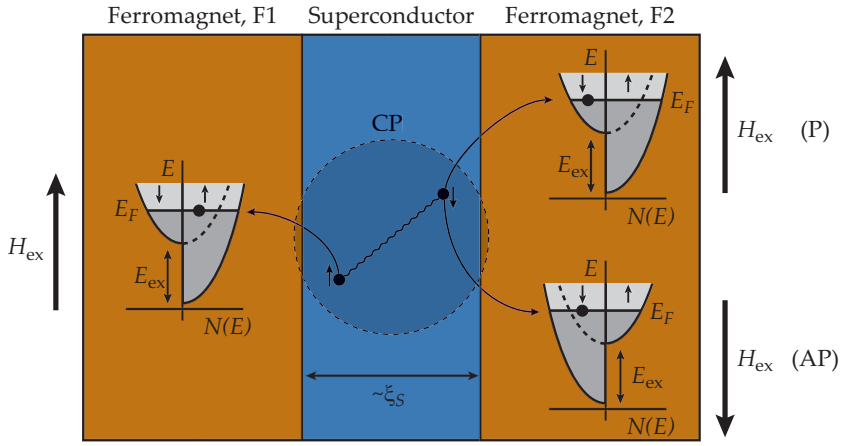

Figure 5.1: Comparing the parallel (P) and anti-parallel (AP) configuration of the ferromagnetic exchange fields H_{ex} in a superconducting spin-valve. Here, a Cooper pair (CP) couples the two ferromagnetic layers F1 and F2, with ξ_S the superconducting coherence length. In F1 the orientation of H_{ex} is "down" while in F2 the orientation is either "up" (AP configuration) or "down" (P configuration). The presented electron band structures represent strong ferromagnets with non-zero polarization.

A crossover from the established weak limit result to a reversal of the effect for strongly spin polarized ferromagnets is thus expected, but no theoretical predictions nor experimental data are available to confirm or refute this. To complicate matters, a relative increase of resistance when switching the magnetization may also be due to a change in the stray fields coming from the F layers. These issues are reflected in the literature. Results obtained on weak ferromagnet based spin-valves are all in line with the theoretical predictions, but that is not the case for systems involving strong magnets, such as Ni [50], $Ni_{80}Fe_{20}$ (Permalloy, Py) [51, 52, 53], Co and Fe combined [54] or Co [55]. In a number of these experiments, a *reversed* behavior is observed, giving a higher T_c in the parallel alignment. This is the case in reports on Nb/Py[51, 53], Nb/(Co,Fe)[54] and Nb/Co[55]. What all these reports have in common is that they do not make use of an anti-ferromagnetic pinning layer to pin the magnetization direction of one of the two F layers. The other experiments using strong ferromagnets all *do* use such pinning layer, improving the qual-

ity of the AP state, and there the "standard" spin-valve working is obtained. The non-pinned devices make use of F layers which intrinsically have different switching fields in order to switch them separately and create the AP alignment. This can be obtained by using different materials or thicknesses for the two F layers. The reports showing the reversed behavior do not agree on the suggested dominant mechanism, although most are in favor of a stray field based explanation, which in weak ferromagnetic based spin-valves was shown not to be (dominantly) present at all. A plausible argumentation is that the absence of a (strong) pinning layer (the switch field for the pinned AFM layer is quite a bit higher than the switch field of the F layer) leads to a less well defined AP state, where domains are present. The dipolar fields coming from these domains then have to overpower the effect of exchange field averaging, which is the standard (weak limit) mechanism. This fits with the following reports, which are all based on macroscopic sized samples. In the work of Stamopoulos *et al.* [53] a stray field coupling between the F layers is claimed, which act as source for the reversed behavior. In the work of Steiner *et al.* [54] it is concluded that the results strongly favor an explanation based on local stray fields. In the work of Carapella *et al.* [55] it is claimed that stray fields create a glassy vortex state, which is responsible for the reversal. A different mechanism connected to the polarization of the spin bands was claimed by Rusanov *et al.* [51] who used microscopic sized samples and was the first to observe this reversal. For such small samples, a deviant working of the device is not unexpected due to the lateral sizes competing with domain formation and switching.

To determine the T_c shift one typically measures the transition curve $R(T)$ from normal to superconducting state, and compares the P and AP alignments (preferably at equal but opposite external field). To gain more insight in the working of the device, a full field sweep at a fixed temperature on the transition curve can be made. The resistance ideally would remain constant until the device switches states, at which the resistance jumps to its different value. Especially in the work of Rusanov *et al.* [51] such (almost perfect) jumps/blocks where found and it was assumed this was directly related to a switching between the states (P and AP). However, the lowest resistance (highest T_c) was found in the P configuration, meaning a reversed result compared to the weak limit result. In this work we re-examined this issue.

Here we present a series of measurements on Nb/Py bilayers and spin-valve devices where we compare anisotropic magnetoresistance (AMR) effect in the normal state with the magnetoresistance measurements in the superconducting

state. We also present measurements of the depairing (critical) current I_{dp} far below T_c, and we explore both large scale devices (which were commonly used in previous works) and micro-sized devices. In particular we show that a dipolar coupling between the two Py layers disturbs the AP configuration in the spin-valve, and that the suppression of the stray fields outweighs the domain averaging effect of Cooper pairs.

5.3 Experimental details

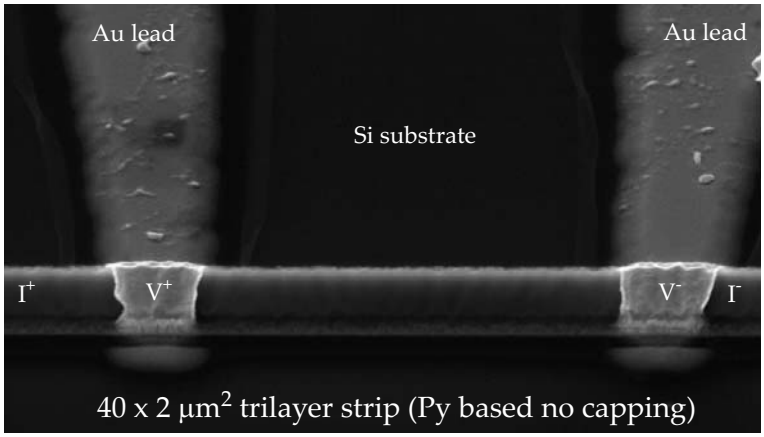

Figure 5.2: SEM image of a 4-probe 40×2 μm^2 spin-valve device. The distance between the voltage probes (V^+ and V^-) is 10 μm and the full length of the spin-valve wire is 40 μm. Similar Au contacting leads for the current probes are at the end points of the wire (not shown).

Nb/Py layers were grown on Si(100) substrates by DC magnetron sputtering in a ultra high vacuum chamber with a background pressure of 10^{-9} mbar and an Ar pressure of 4 μbar for the Nb and 2.5 μbar for the Py, with Nb as bottom layer (see Ch. 3.1 for additional details). The substrate holders were equipped with a small magnet to determine the direction of easy axis for the Py layers and enhance the fast switching properties. The Nb layer thickness was kept at 50 nm for all samples, while for the Py layers thickness we used 20 nm and 50 nm. For our Py/Nb/Py spin-valve devices the bottom Py layer is 50 nm thick and the top Py layer is 20 nm thick. All devices have an additional 2 nm Nb capping layer added on top to prevent oxidation of the top Py layer. In Ch. 5.4.4 we show that not adding such a protective layer leads to a exchange-biased Py layer, likely due to anti-ferromagnetic iron-oxide formation. The Py has a degree of polarization close to 45 % and

a Curie temperature around 900 K. The purity of the Nb target is 99.95 % which yields a T_c of 9.1-9.2 K. Standard electron beam lithography was used to pattern both the micro-sized strips, with a length of 40 μm and a width of 1 to 4 μm, and the large scale devices (2000×200 μm^2). In all cases, the direction of the strips is aligned with magnetic easy axis of the Py layer. The strips were etched using Ar ion-etching at an Ar pressure of 3 μbar with a background pressure of 10^{-6} mbar. Au contacts were sputtered in a second deposition step using a lift-off resist mask technique. A few nanometers of Ti were sputtered as adhesion layer for the Au. The contact geometry is 4-probe, with 10 μm spacing between the voltage probes for the micro-sized strips and 1000 μm for the large scale structures. Fig. 5.2 shows a SEM (scanning electron microscope) image of a 40×2 μm^2 spin-valve. This recipe is used for both bilayer and spin-valve, both for micro-sized and macro-sized devices. Typical

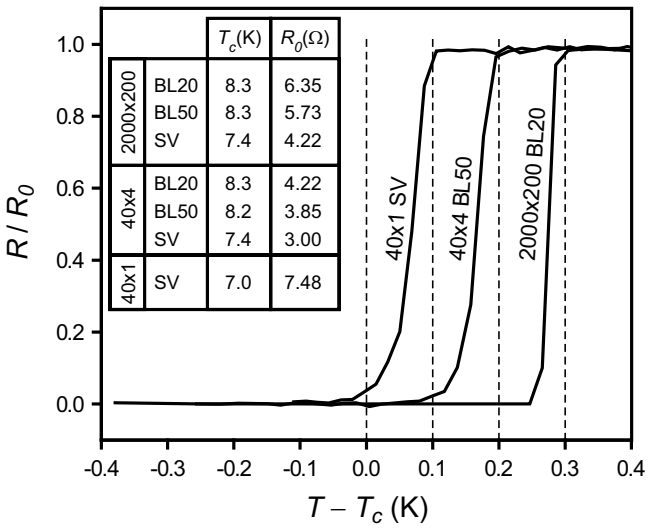

Figure 5.3: Temperature variation of the resistance around the transition temperature T_c (plotted as $T - T_c$) for (from left to right) a Py(50)/Nb(50)/Py(20) spin-valve (SV), a Nb(50)/Py(50) bilayer (BL50) and a Nb(50)/Py(20) bilayer (BL20), with numbers representing the layer thickness in nm. Resistance is normalized to the low temperature resistance R_0 and curves are shifted along temperature for clarity. Lateral dimensions of the devices are given in the graph in units of μm^2. The table shows T_c and R_0 of all devices presented in this chapter.

transition curves (resistance R versus temperature T around T_c) for several of our devices are shown in Fig. 5.3, where curves are represented as $T - T_c$ (with T_c defined as the midpoint of the transition) and shifted for clarity. The

typical width of the transition is 50 to 100 mK. Also shown in the figure are all T_c's and low temperature normal state resistances (R_0) for our devices. Note the difference in T_c between bilayers and spin-valves. The choice for the different layer thicknesses for the Py in the spin-valve device is to establish different coercive fields, making the device switchable from parallel to anti-parallel. The coercive fields of the 20 and 50 nm thick micro-sized Py strips are expected to be in the range from 0 to 20 mT [51] with a wider strip leading to a lower coercive field value (a large Py thin film of 20 nm thickness was measured to have a coercive field less than 0.5 mT). For our typical micro-sized strips (1 to 4 μm wide) we have always found a difference of about 5 mT between the two different thicknesses. However, as we will show later, the mutual influence of the exchange fields prevents a clean switching. The micro-sized elongated structures were chosen to promote single domain switching. They also have sufficiently large cross-sectional resistance to perform critical current (I_c) measurements. We performed anisotropic magneto-resistance (AMR) measurements (mainly at low temperature) just above T_c to see if and when domains appear in our Nb/Py bilayer systems, and then compare this to the AMR signal of the trilayer to see if the Py layers become coupled through their dipolar fields. The response of the superconductor is found by comparing these AMR measurements to the magnetoresistance measurements in the transition. All measurements were done in a standard ^{4}He cryostat with magnetic shielding to provide a low-noise environment. It is equipped with a superconducting coil to generate magnetic fields up to 1 T. All field measurements are performed with the direction of the applied field H_a along the long side of the strip, which implies $H_a \parallel I$ (the measurement current). The critical current (I_c) measurements are performed well below T_c, and probe the gap strength, enabling a comparison between P and AP below the transition area. A pulsed current method was used for these measurements, which is described in Ref. [59].

5.4 Results

5.4.1 $R(H)$ for $T > T_c$

Fig. 5.4 shows the result of $R(H)$ measurements on large scale Nb/Py bilayers and a Py/Nb/Py spin-valve, all with lateral dimension 2000×200 μm^2 and at a temperature of 9 K (Nb in normal state). All devices show the characteristic AMR dip, with a relative resistance change close to 0.06 percent. The spin-valve and bilayer with the thick Py layer (50 nm) show a very similar hysteretic curve with a coercive field value close to 1 mT, however, the bilayer with the thin Py layer (20 nm) shows a much broader dip with a coercive field close

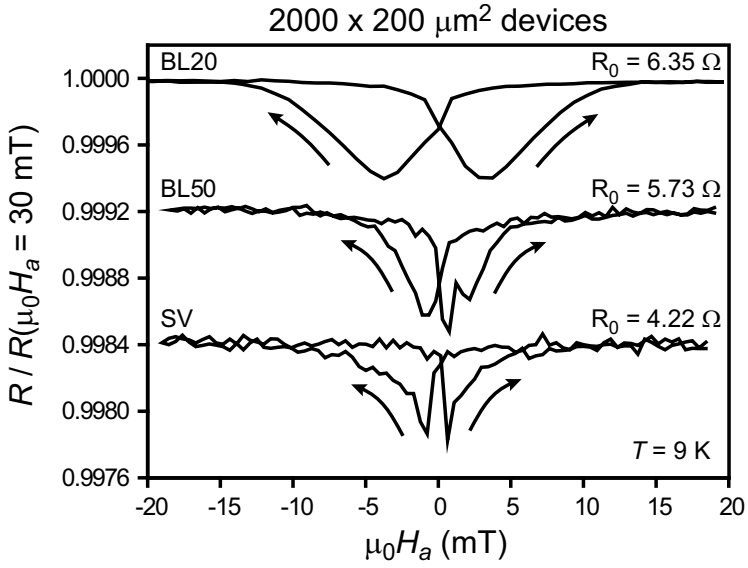

Figure 5.4: Resistance normalized to the value at 30 mT (called R_0 in the figure) as function of the in-plane applied field H_a on large scale devices with lateral dimension 2000×200 μm^2, all at temperature $T = 9$ K. From top to bottom, a Nb(50)/Py(20) bilayer (BL20), a Nb(50)/Py(50) bilayer (BL50), and a Py(50)/Nb(50)/Py(20) spin-valve (SV), with numbers representing the layer thickness in nm. The BL50 and SV curves are shifted by respectively -0.0008 and -0.0016.

to 3 mT. The same measurements but now on micro-structured strips, all with lateral dimension 40×4 μm^2, are shown in Fig. 5.5. For the spin-valve, block-shaped hysteretic dips appear with switches near ±1 mT and ±3 mT, and with (again) a relative resistance change of 0.06 percent. For both the 50 nm thick and 20 nm thick bilayer we do not see any AMR dip coming out of the measurement noise, pointing towards a single domain type of switching. The noise level is similar for all three devices and about 0.01 percent, which is 0.3-0.4 mΩ in terms of absolute resistance value. It is significantly worse than the large scale devices and suggests that contacts to the strip are of lesser quality.

The appearance of this (seemingly) 2-step switch process in the micro-sized spin-valve is very different from the large scale spin-valve. Yet, the size of the resistance chance is similar in both cases, and the observed switching fields of the blocks coincide with the coercive fields of the two different large scale bilayers (1 mT and 3 mT, respectively). To further explore this 2-stepped type

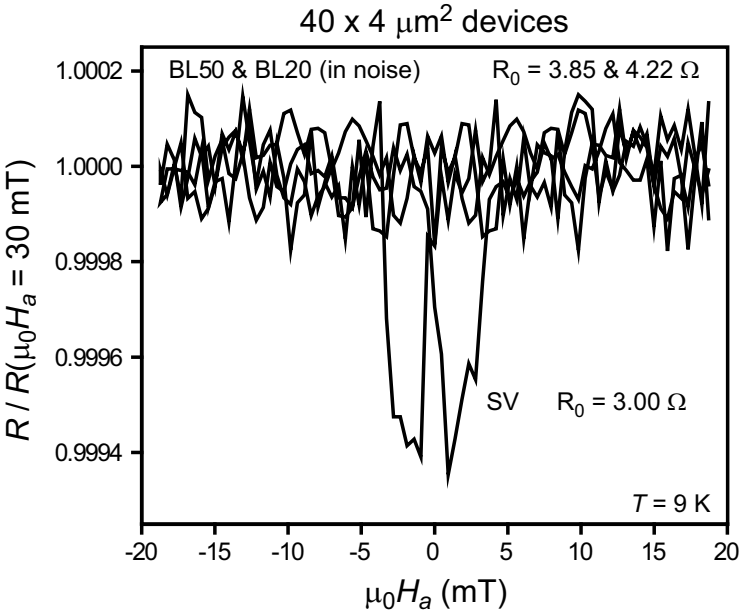

Figure 5.5: Resistance normalized to the value at 30 mT (called R_0 in the figure) as function of the in-plane applied field H_a on micro-sized devices with lateral dimension 40×4 μm^2, all with temperature $T = 9$ K. The presented curve is from a Py(50)/Nb(50)/Py(20) spin-valve, while the results on the Nb(50)/Py(20) and Nb(50)/Py(50) bilayers (BL20 and BL50) are "flat" and within the noise of the spin-valve, with numbers representing the layer thickness in nm.

of switching we fabricated a narrower bridge (1 μm wide) increasing the shape anisotropy energy, thus enhancing its importance in determining the possible domain states in the strips. Results are presented in Fig. 5.6 and show a series of $R(H)$ measurements at constant temperature ($T = 9$ K) above T_c. Although no two curves are identical, there seem to be only a limited number of values for the applied field where a jump in resistance is seen, and also the size of those jumps take only few different values. The range over which hysteresis is found goes from $\pm$ (4 to 14) mT, which is significantly higher than in the other devices. Also the size of the resistance change is about $10\times$ higher than in our wider devices, implying more dense, and/or more perpendicular domains (perpendicular to the current direction).

In all the large scale devices (bilayer and spin-valve) domains appear during the switching, with a lower coercive field for a thicker Py layer. However,

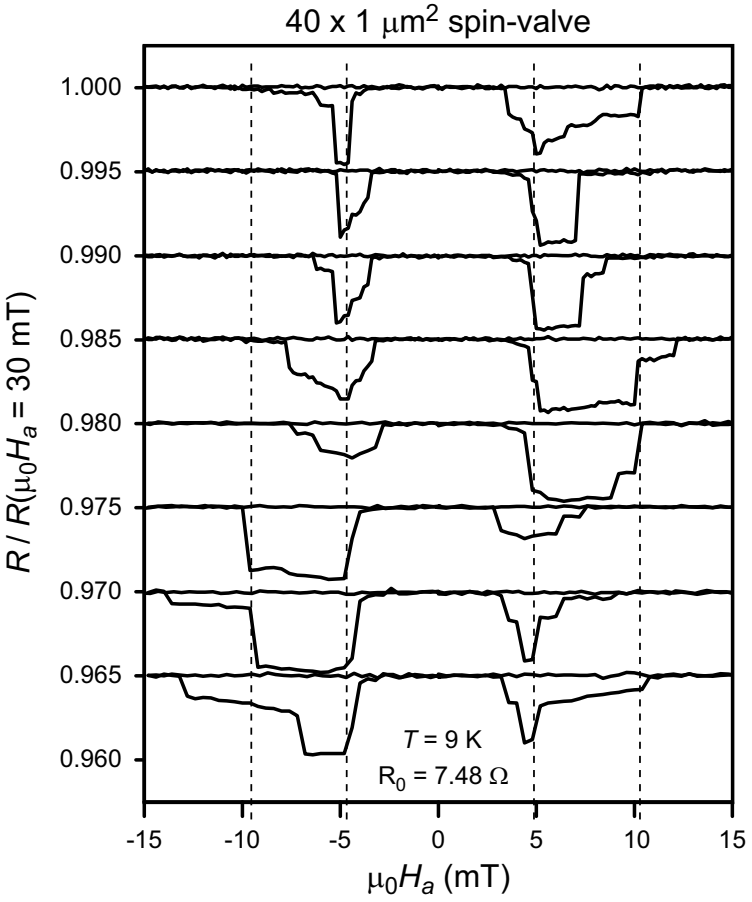

Figure 5.6: Resistance normalized to the value at 30 mT (called R_0 in the figure) as function of the in-plane applied field H_a on a 40×1 μm^2 Py(50)/Nb(50)/Py(20) spin-valve, with numbers representing the layer thickness in nm. All curves have a different magnetic history and are repeatedly shifted by -0.005. For all measurements the temperature was 9 K.

while the F layers in the bilayer devices can apparently switch freely, they evidently become magnetically coupled in the spin-valve device. This coupling appears to be such that a switching in the thinner layer (highest coercive field) is triggered by the switching of the thicker layer (lowest coercive field). In the 40×4 μm^2 bilayer strips, the switching is no longer accompanied by the formation and movement/rotation of domains over a relative broad field range, but rather makes a fast single switch. Most likely this is due to the enhanced shape anisotropy which favors single domain switching. In a spin-

valve device of the same lateral dimension the F layers become coupled, just as in the large scale spin-valve. Only now, the intrinsic type of switching of the separate layers is different, and this results in a two-stepped switch process for the spin-valve. We recall that a dip in the resistance of the AMR signal (in our devices) is representative for the appearance of inhomogeneities (domains) in the magnetization. Therefore, rather than a switch from parallel to anti-parallel, the blocks in the AMR signal indicate a switch from parallel to a domain state. The measurements on the 40×1 μm^2 spin-valve show that a variety of possible domain states exists, which can be entered during the two-stepped type of switching. In wider strips we have never observed such behavior.

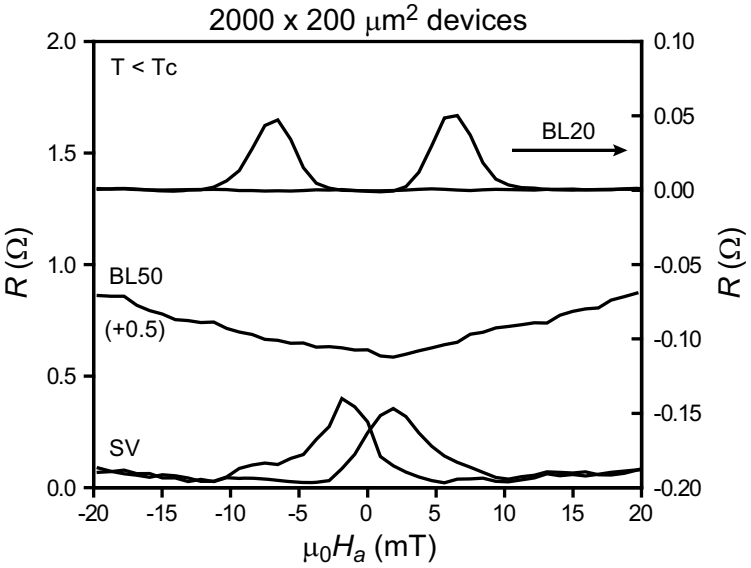

Figure 5.7: Resistance as function of the in-plane applied field H_a on large scale devices with lateral dimension 2000×200 μm^2, at temperatures on the low-end of the transition curve (Nb in superconducting state). From top to bottom, a Nb(50)/Py(20) bilayer (BL20), a Nb(50)/Py(50) bilayer (BL50) and a Py(50)/Nb(50)/Py(20) spin-valve (SV), with numbers representing the layer thickness in nm. The BL50 curve is shifted by +0.5 and the BL20 curve is on the right-hand scale.

5.4.2 $R(H)$ for $T < T_c$

A similar set of measurements is performed inside the transition, with Nb superconducting. The $R(H)$ are all taken at temperatures near the low-end

of the transition curve to improve temperature stability. The measured signal now comes predominantly from the superconductor which is shorting the ferromagnetic layers by percolation paths. Furthermore, any AMR features are no longer visible due to the (relative) high $\partial R/\partial T$ in the transition. Our typical 100 mK transition width, combined with a 10^{-4} relative resistance change corresponds to a temperature change of 0.01 mK, which is below our measurement accuracy of about 0.3 mK. Fig. 5.7 shows the result of $R(H)$

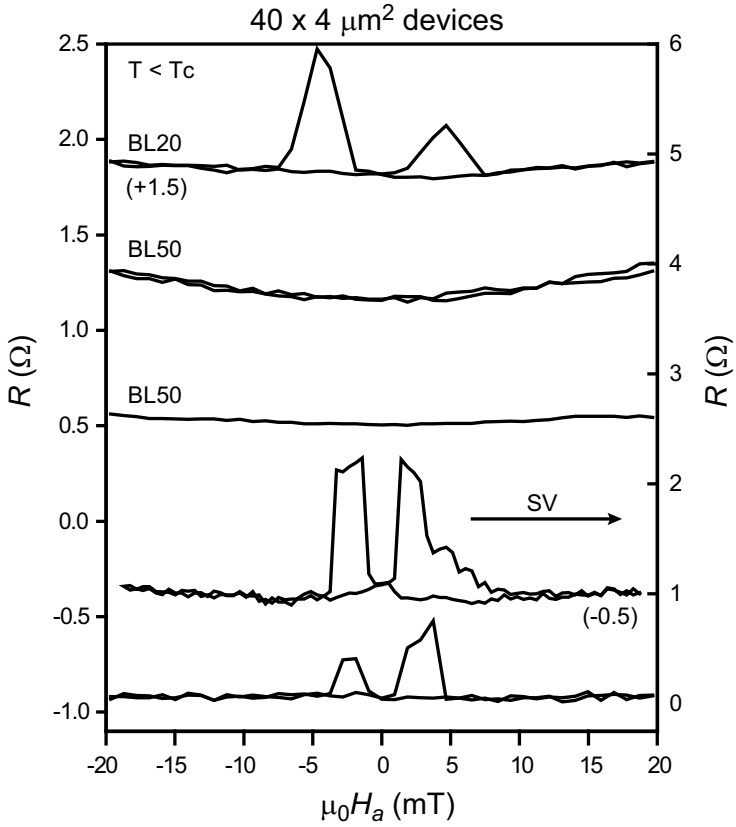

Figure 5.8: Resistance as function of the in-plane applied field H_a on micro-sized devices with lateral dimension 40×4 μm^2, at temperatures on the low-end of the transition curve (Nb in superconducting state). From top to bottom, a Nb(50)/Py(20) bilayer (BL20), 2x a Nb(50)/Py(50) bilayer (BL50), and 2x a Py(50)/Nb(50)/Py(20) spin-valve (SV), with numbers representing the layer thickness in nm. Two curves are shifted (by -0.5 and +1.5) as indicated. The SV curves are on the right-hand scale.

measurements on the large scale devices (2000×200 μm^2). While the bilayer with the 50 nm thick Py layer does not show any hysteric feature at all, the

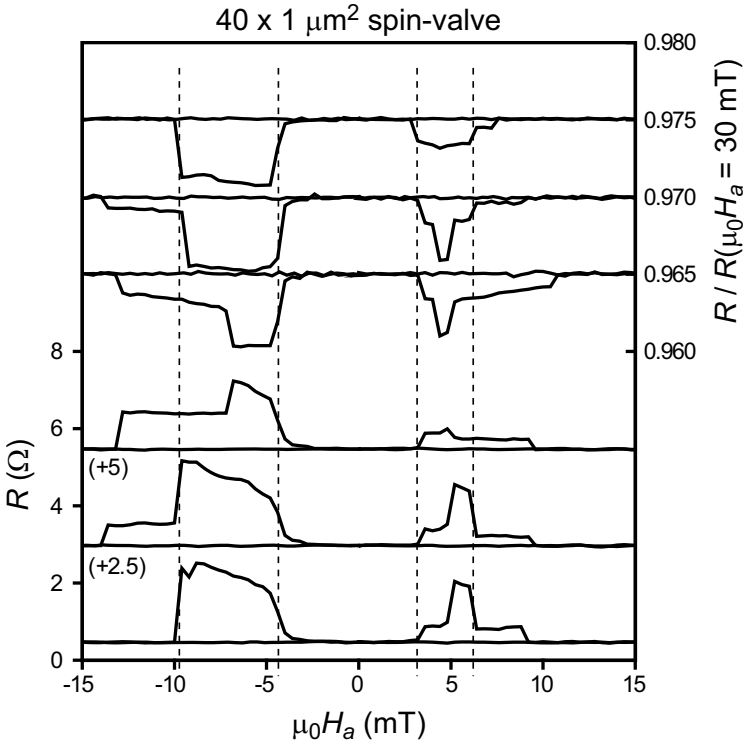

Figure 5.9: Comparison of the resistance as function of the in-plane applied field H_a on a 40×1 μm^2 Py(50)/Nb(50)/Py(20) spin-valve (numbers representing the layer thickness in nm) between temperatures on the low-end of the transition curve (Nb in superconducting state) and above the transition temperature T_c (Nb in normal state). All curves have a different magnetic history. Left-hand scale: results for $T < T_c$ with curves repeatedly shifted by +2.5 as indicated. Right-hand scale: results for $T > T_c$ taken from Fig. 5.6.

bilayer with the 20 nm thick Py layer shows clear hysteric peaks. The location of these observed peaks are around ± 6 mT, which is significantly higher than the corresponding AMR dips (in the same device) which are at ± 3 mT. Also the spin-valve shows such hysteretic peaks, but located at lower fields around ± 2 mT (the corresponding AMR dips in the same device are at ± 1 mT). For the micro-sized devices (40×4 μm^2) the same trend is observed (see Fig. 5.8) with again no hysteretic feature in the bilayer with the 50 nm thick Py layer, while the bilayer with the 20 nm thick Py layer and the spin-valve both do show hysteretic peaks. In case of the bilayer, the peaks are located at ± 4 mT (a lower value compared to the large scale devices) and still resemble the shape

of peaks. For the spin-valve the peaks are now really block-shaped, indicating again a 2-stepped type of switching, and have switching fields at ± 1 mT and ± 4 mT. In Fig. 5.9 we present the $R(H)$ measurements on the thinner spin-valve (40×1 μm^2), and make a direct comparison with the obtained $T > T_c$ results (of the same sample, see Fig. 5.6). Block-shaped peaks are observed with switches at ± 4 and ± 10 mT (or ± 14 mT) . Furthermore, there is a striking resemblance between the observed blocks for $T > T_c$ (dips) and $T < T_c$ (peaks). All observed switching fields in the $R(H)$ measurements on the large scale and micro-sized devices are collected in Table I:

	2000 × 200			40 × 4			40 × 1
	SV	BL50	BL20	SV	BL50	BL20	SV
$T > T_c$	1	1	3	1-3	-	-	4-14
$T < T_c$	2	-	6	1-4	-	4	4-14

Table I: Switching fields in mT for the various structures and samples, both above and below T_c.

5.4.3 $I_c(H)$ for T well below T_c

The presented transport measurements so far, all focus on temperatures closely around the transition ($T \sim T_c$). To study the working of the spin-valve well below T_c we conducted a series of critical current measurements as function of applied field, $I_c(H_a)$ by measuring the current I - voltage V characteristic. We used 3 ms current pulses, with an interval of several seconds and increasing in amplitude until the critical current is reached and the superconductor is driven in the normal state. The sample is initially cooled down in zero field condition and the first measurement at a fixed temperature always starts in zero applied field. The obtained I-V curves all showed a sharp jump from almost zero voltage to the normal state, which indicates that we are measuring a depairing current rather than the onset to vortex flow. This we (consistently) found before on S-films and S/F bilayers [59, 57, 68]. The measurement is thus directly sensitive to the amplitude of the superconducting gap, which limits the critical current. Additionally, the value of I_c is well defined due to the sharp transition. The results for the 40×4 μm^2 Nb/Py spin-valve are shown in Fig. 5.10, where $I_c(H)$ curves are presented at four temperatures well below T_c, which, in terms of the reduced temperature $t = T/T_c$ go down to $t = 0.5$. All data show a block-like dip for the increasing applied field (coming from negative saturation) with switching fields around 0.5 mT and 3.5 mT, after which the curve becomes constant. The observed switching fields of the blocks do not show a temperature dependence, but do show a diminishing effect for

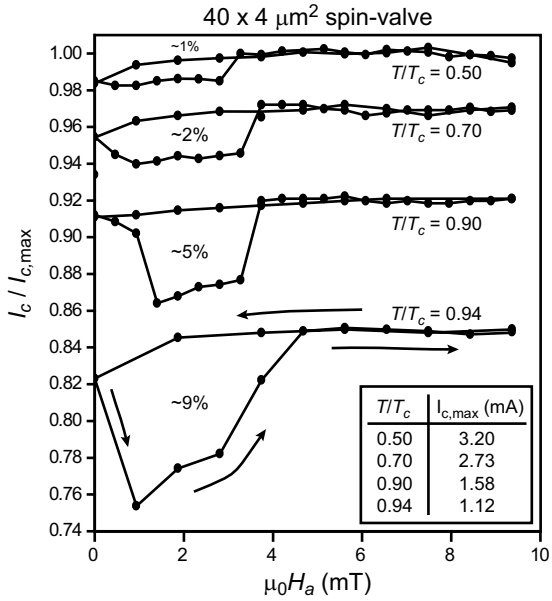

Figure 5.10: Critical current measurements I_c, normalized to the maximum observed value $I_{c,\max}$ per temperature, as function of the in-plane applied field H_a on a 40×4 μm^2 Py(50)/Nb(50)/Py(20) spin-valve. The curves represent different reduced temperatures T/T_c and are shifted for clarity by -0.03, -0.08 and -0.15. The indicated percentages are the relative sizes of the dips.

decreasing temperature. The uncertainty in the determination of I_c is about the step size for the increase in current (1 μA). We interpret the decrease of I_c in the hysteretic region as a suppression of the superconducting gap. Because the gap increases in strength for lower temperature, it is not strange to see a diminishing effect of the percentage change. The switching fields coincide with the values found in the transport measurements close to T_c (see Fig. 5.5 and Fig. 5.8). Fig 5.11 shows the $t = 0.94$ curve up to higher field values, and the standard decrease of I_c due to applied field becomes visible. Additionally, the inset shows the actual I - V measurement at the highest used field (125 mT).

5.4.4 Exchange biased Py

All presented data so far has been on devices where the top Py layer is covered by a thin Nb layer to protect it from oxidizing. Magnetoresistance measurements on a 40×2 μm^2 bilayer strip *without* such capping layer are presented in Fig. 5.12, where $R(H)$ at room temperature ($T = 300$ K) is compared with

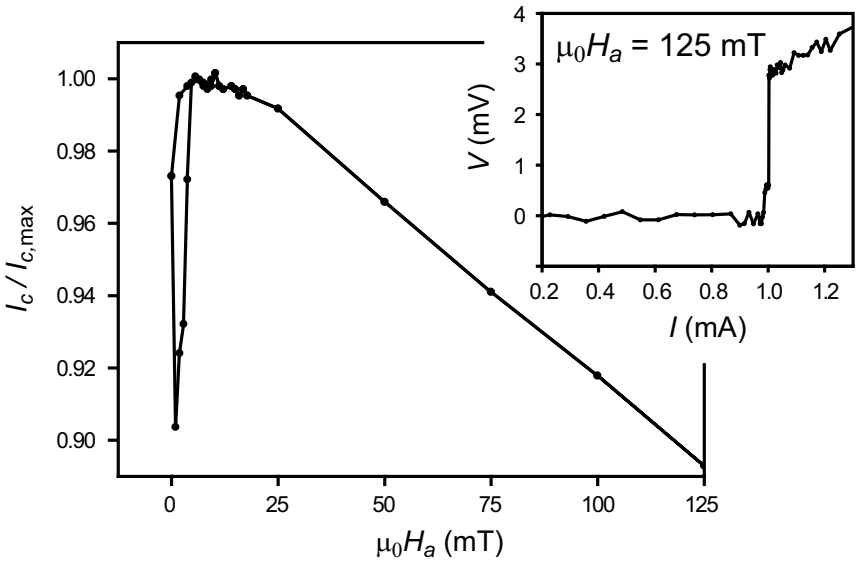

Figure 5.11: High field behavior of the $T/T_c = 0.94$ critical current measurement as presented in Fig. 5.10. The inset shows the current voltage measurement of the curve for $\mu_0 H_a = 125$ mT.

low temperature ($T = 10$ K). At room temperature the AMR signal contains the typical dips. They are symmetrical around zero field, with a coercive field of $\pm$ 6 mT, and with a relative resistance change of 0.005. At low temperature the dips have become broader, the coercive fields have become larger, but the curve is no longer symmetric around zero field. The coercive fields are now at -14 mT and 9 mT, which indicates an exchange bias of 2.5 mT (such that unbiased the coercive fields would be symmetric again at $\pm$ 11.5 mT). We expect this exchange bias to be the result of the formation of anti-ferromagnetic Fe_2O_3 in the Py layer.

5.5 Discussion and conclusion

Combining the results from all measurements above, the data sketch a coherent picture of the behavior of Py/Nb/Py spin-valve structures. For temperatures *above* the transition (Nb in normal state) we find that the resistance changes are dominated by the AMR effect of the Py layers, with a relative resistance change of order 10^{-4}. In large scale devices, where domain formation is not limited by the size of the sample, the observed resistance dips in the bilayers with 20 nm and 50 nm thick Py appear at different fields. For the spin-

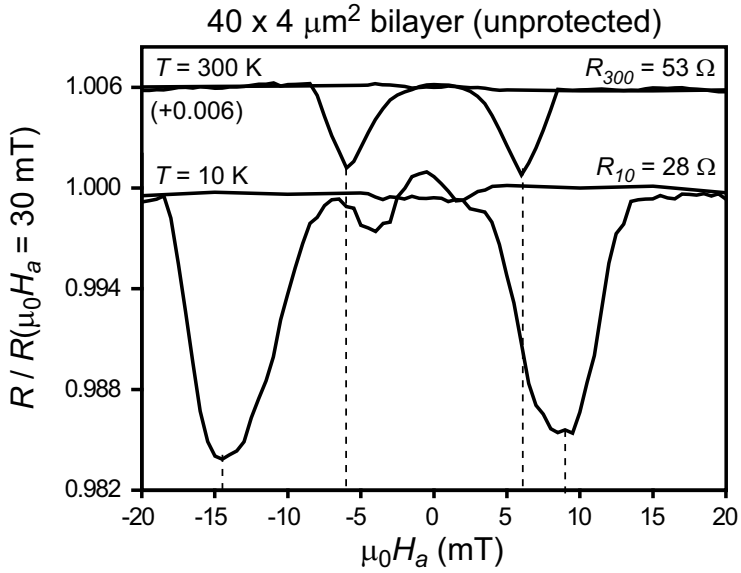

Figure 5.12: Resistance normalized to the value at 30 mT as function of the in-plane applied field H_a on a 40×4 μm^2 Nb/Py bilayer, for $T = 300$ K and $T = 10$ K. The respective resistances are indicated by R_{300} and R_{10}. Both the Nb layer and Py layer are 20 nm thick.

valve structure we then expect to see all four resistance dips in the AMR, however, we observe a behavior very similar to the bilayer with 50 nm thick Py. Going to the microscopic regime, we no longer observe any dips at all in the AMR signal of the bilayers, pointing towards a fast single domain type of switching. Surprisingly, in the spin-valve we *do* observe resistance changes in the AMR signal. A 2-stepped switching has appeared by going from large scale to micro-sized spin-valves, most strongly pronounced in the thinnest (1 μm wide) spin-valve structure. We believe this is a strong indication for a magnetic coupling between the two Py layers by dipolar/stray fields, which are locking domains into a (meta)stable configuration. For temperature *below* the transitions (Nb superconducting) we observe peaks in the resistance now dominated by changes in the superconducting gap, with a relative resistance change of order 10^{-1}. Especially in the 1 μm wide spin-valve, these peaks are mirror images of the dips in the corresponding AMR signals. This implies that 1) the superconductor does not influence/change the switching behavior of the spin-valve, and 2) suppression of the superconductor is a direct effect of the presence of the stray fields connecting the two Py layers. Such coupling between the two F layers has not been found in any of the experiments using

antiferromagnetic pinning layers. In the bilayers we only observe these peaks in the devices with 20 nm thick Py (and not in the devices with 50 nm thick Py). This we attribute to different types of domain walls. It is known that for very thin Py layers the domain wall becomes of the Néel type, while for thicker Py layers it is Bloch type [69]. The crossover between the two is around a Py thickness of 35 nm, implying Néel walls in our 20 nm thick Py bilayer and Bloch walls in our 50 nm thick Py bilayers. Calculations on stray fields generated by domain walls shows a significantly higher magnitude for Néel walls than for Bloch walls [70], which we believe is the source of the observed difference in our bilayers. No traces are found of an enhancement of the superconductivity by domain averaging from Cooper pairs, which we *did* observe in our CuNi based devices and is the established weak limit result. We thus conclude that the stray field contributions coming from the domains dominate over this averaging effect. By going to lower temperatures and measuring the critical current, which is a direct measure for the superconducting gap strength, we observe that the suppression of superconductivity is still present. The fields at which the suppression occurs overlaps with the peaks in the magnetotransport measurements and do not change with temperature. This indicates that also a well developed gap is not changing the switching of the Py layers, and likely the spin-valve is still dominated by the stray fields. In our I - V measurements we do not see traces of a vortex flow, while the stray fields connecting the two F layers should result in vortices. However, since the domain state seems to be unaffected by the gap, we believe it strong enough to keep any vortices in place. Effectively, all vortices generated by the stray fields are strongly pinned by the (rigid) domain state itself.